Coordination Chemistry Reviews 557 (2026) 217754

Contents lists available at ScienceDirect

Coordination Chemistry Reviews

journal homepage: www.elsevier.com/locate/ccr

Monovalent ions aid catalysis of two-metal-ion dependent RNA editors☆

Jure Borišek [a,*], Jana Aupič [b], Alessandra Magistrato [b,*]

[a] Theory Department, National Institute of Chemistry, Ljubljana 1001, Slovenia
[b] CNR - Istituto Officina dei Materiali (IOM) at International School for Advanced Studies (SISSA), 34136 Trieste, Italy

ARTICLE INFO

Keywords:
Two-metal-ion catalytic mechanism
Monovalent metal ion
Phosphodiester bond cleavage
QM/MM simulations
Spliceosome
Ribonuclease

ABSTRACT

The cleavage and formation of phosphodiester bonds in nucleic acids is performed by diverse cellular machineries ranging from small protein enzymes to large complexes composed of proteins and/or RNA strands. While it has long been believed that these processes depend solely on a two-metal-ion mechanism, comparative structural analyses revealed that some complexes also contain highly conserved second-shell monovalent cations. The two-Mg^{2+}-aided catalytic mechanism, in which both ions function as Lewis acids, with one metal activating the nucleophile (water or ribose hydroxyl) for the scissile phosphate group attack and the other stabilizing the leaving group, is well-established. In contrast, the function of monovalent ions has been largely overlooked, yielding divergent results across different catalytic settings. Nevertheless, recent evidence points to monovalent ions assisting catalysis beyond their roles in RNA folding and assembly. Here, building on recent computational studies on two-metal-ion dependent ribozymes, we showcase how divalent and monovalent ions finely tune the catalytic site arrangements and dynamics, affecting the kinetic and thermodynamic properties of RNA cleavage reactions. We discuss optimal catalytic mechanisms depending on nucleophile type and illuminate strategies adopted by second-shell monovalent ions to optimize catalytic geometries, which enable efficient proton transfer from nucleophile to the leaving group, a key event for effective catalysis. This review expands understanding of nucleic acid-processing machinery, providing key knowledge for potentially designing innovative gene-modulating tools and therapeutic strategies.

1. Introduction

The processing of nucleic acids represents a cornerstone of molecular biology, encompassing fundamental reactions such as DNA replication and repair, RNA transcription, splicing, translation and degradation [1]. These reactions, which involve the cleavage and formation of phosphodiester bonds, are catalyzed by a diverse array of enzymes, including protein-based polymerases and nucleases as well as RNA-based ribozymes and protein/RNA-based ribonucleoproteins (RNPs). A remarkable feature shared across many of these evolutionarily distinct machineries is their reliance on divalent metal ions as essential catalytic cofactors [2,3].

A unifying mechanistic framework for many of these enzymes was proposed in 1993 by Steitz and Steitz, who postulated a general two-metal-ion mechanism for phosphoryl transfer reactions [4]. This model posits that two divalent metal ions, typically Mg^{2+}, are positioned in the active site to orchestrate catalysis. One ion (M1) acts to lower the pKa of the attacking nucleophile, either a water molecule or a (deoxy) ribose hydroxyl, while the second ion (M2) stabilizes the developing negative charge on the pentacovalent phosphorane-like transition state and the leaving group [4,5]. This elegant and powerful hypothesis provided a chemical rationale for the observed metal dependence of numerous nucleic acid processing enzymes and predicted that ribozymes would converge on a similar catalytic solution as their protein counterparts.

Subsequent decades of structural and biochemical research have confirmed this model. The two-metal-ion catalytic core was first visualized in the active sites of different DNA and RNA polymerases, RNase H, and *exo*- and *endo*-nucleases [6,7]. A landmark crystal structure of group I self-splicing introns in 2005 provided the first direct structural evidence of a two-metal-ion catalytic center also in a ribozyme, supporting the predicted evolutionary convergence [8]. Since then, this motif has been identified in the active sites of other ribozymes, including group II introns that catalyze pre-mRNA splicing in bacteria [9], in engineered polymerase ribozymes [10], and large protein-directed ribozymes such as the spliceosome, which catalyzes pre-mRNA

☆ This article is part of a Special issue entitled: 'TDTilley-70' published in Coordination Chemistry Reviews.

* Corresponding authors.
E-mail addresses: jure.borisek@ki.si (J. Borišek), alessandra.magistrato@cnr.it (A. Magistrato).

https://doi.org/10.1016/j.ccr.2026.217754
Received 28 January 2026; Received in revised form 12 February 2026; Accepted 19 February 2026
Available online 25 February 2026

splicing in eukaryotes [11–13], ribonuclease P, which catalyzes the maturation of the 5′-end of precursor transfer RNA (pre-tRNA) [14] and ribonuclease MRP, which processes pre-ribosomal RNA [15].

The active sites of these (ribo)enzymes are highly negatively charged, and additional metal ions and/or basic amino acid residues were thought to contribute to reducing the electrostatic repulsion of the phosphate backbone [16]. As such, monovalent cations like K^+ and Na^+, while known to be essential for the folding and structural stability of large RNAs [11,17], were largely considered to be background electrolytes with no specific catalytic function [18,19].

Despite the success of the two-metal-ion model, it has recently become apparent that it may not fully capture the complexity of the catalytic environment of nucleic acid processing machineries [20,21]. A re-evaluation of ribosome crystal structures highlighted the prevalence and specificity of monovalent ion binding in large RNAs [22]. Moreover, structural studies demonstrated the relevance of monovalent ions in ribozymes [16]. More recently, and of direct catalytic relevance, cryo-EM [20] and computational [23] studies demonstrated the presence of a conserved and functionally critical K^+ ion in the immediate vicinity of the two catalytic Mg^{2+} ions in the spliceosome active site. This discovery suggests that the canonical two-metal-ion mechanism can be augmented by second-shell monovalent cations that actively participate in catalysis.

Understanding the synergistic interplay between divalent and monovalent ions presents a challenge. Their distinct chemical properties, with Mg^{2+} being a small, strong Lewis acid favoring specific inner-sphere coordination versus K^+ being a larger, softer ion with more flexible coordination, suggest they fulfill complementary roles. Elucidating this intricate ionic effect is crucial for a complete understanding of RNA processing. However, the exact experimental assignment of divalent and monovalent ions in RNA structures remains particularly challenging [22].

In this review, we explore the catalytic mechanisms of two-metal-ion dependent RNA processing machineries, with a particular focus on the multi-metal ion framework. First, computational methods and the core principles of the canonical two metal ion mechanism and its variations are revisited, followed by emerging evidence for specific roles of monovalent ions in catalysis. Throughout, we provide general mechanistic considerations and guidelines based on the combined effects of these ions.

2. Computational simulation methods

Computational methods, particularly all-atom classical molecular dynamics (MD) and hybrid quantum mechanics/molecular mechanics (QM/MM) simulations, have the capability to examine reaction mechanisms at subatomic details [24], and have thus emerged as a valuable tool for refining the metal center composition, geometry and dynamics, and for dissecting the mechanisms of these complex systems [13,25,26].

Classical MD simulations are the most frequently used technique for investigating the time dependent behavior of biomolecular systems. In this approach, the system is usually modeled at the atomic level, where every atom is treated as a distinct particle with specific mass and charge properties. Rather than calculating complex electronic behaviors, the forces driving the system are estimated using empirical parameters known as force fields. These approximate physical interactions use harmonic functions for bonds and angles, alongside non-bonded terms for electrostatics and van der Waals forces. The simulation proceeds by iteratively solving Newton's equations of motion, typically within a box containing explicit water molecules and ions to mimic physiological conditions [27].

The reliability of MD simulations depends heavily on two factors: the precision of the force fields and the adequacy of conformational sampling [28,29]. Since macromolecular complexes are large and highly dynamic and often undergo structural shifts over hundreds of microseconds to seconds timescales, standard MD simulations may fail to explore their full conformational complexity and landscape. To address this, enhanced sampling methods such as metadynamics [30], umbrella sampling [31], thermodynamic integration [32], and replica exchange methods [33] are often employed. These techniques artificially bias the potential energy surface allowing the system to overcome high energy barriers and access rare conformational states that standard simulations would miss [34,35].

However, classical MD has the fundamental limitation of not modeling electronic structure, and therefore cannot simulate chemical reactions such as bond breaking and formation or charge transfer events involving metal ions [36]. To study the catalytic mechanisms at the heart of enzymes, quantum mechanics (QM) level of theory is required. Since applying high level QM methods to an entire biological complex is computationally prohibitive, a hybrid quantum-classical (QM/MM) strategy is the standard solution [37]. In this setup the reactive center is treated with accurate QM methods while the surrounding environment is handled by the computationally cheaper MM force fields [38]. Defining the QM region correctly is critical as it must encompass all atoms involved in the reaction, including all residues coordinating metal ions and proton shuttling water molecules, to ensure physical accuracy.

QM/MM calculations generally fall into two categories: static and dynamic. Static approaches minimize the energy of the system at specific points along a reaction path, but, while they are computationally efficient, they describe the system at 0 K and therefore ignore entropy. In contrast, QM/MM MD simulations incorporate thermal fluctuations and sample conformational space, enabling calculation of free energy profiles that account for entropic contributions, though at a much higher computational cost [39].

Because QM/MM MD simulations are typically restricted to very short timescales of picoseconds, calculating full reaction pathways requires specific sampling protocols [39]. Thermodynamic integration, alongside metadynamics and umbrella sampling are common techniques used to bridge this gap. In thermodynamic integration, which has been most commonly used in the examples described in the following sections, the reaction coordinate is constrained to specific values and the force required to maintain those constraints is measured and integrated to generate a free energy profile of the chemical reaction [40]. The success of QM/MM MD simulations also rests on the choice of the quantum method. Density functional theory (DFT) approaches, in particular functionals like BLYP or B3LYP, combined with dispersion corrections, have proven effective for modeling phosphodiester bond cleavage and formation in RNA systems [21]. In the few studies where these functionals were directly compared, they were found to yield similar active-site geometries and reaction mechanisms [41]. Consequently, while BLYP is often employed for extended QM/MM MD sampling, B3LYP is used to validate key stationary points or barrier heights. To ensure the reliability of the calculations, it is advisable to first benchmark the chosen quantum mechanical method on small model systems, confirming that it reproduces experimental structural and thermodynamic parameters before extending it to the full biological context.

3. Two-metal-ion mechanism: Core principles

The two-metal-ion mechanism provides a robust and versatile strategy for catalyzing phosphoryl transfer reactions [4], a chemically challenging process due to the electrostatic repulsion between the anionic phosphate backbone and the incoming nucleophile [42]. The core principle of this type of reaction involves the precise geometric arrangement of two divalent cations and their coordinating ligands to cooperatively lower the activation free energy barrier.

The canonical structural arrangement places two Mg^{2+} ions approximately 4.0 Å apart in the (ribo)enzyme's active site, bridged by one of the non-bridging O^{Rp} oxygen atoms of the scissile phosphate [3,4]. In enzymes the octahedral Mg^{2+} ions coordination sphere is completed by aspartates and glutamates, while in ribozymes the metals are cradled by the phosphate backbone. In this configuration, the metal

ions perform distinct yet synergistic roles. As mentioned above, the first M1 metal directly coordinates the attacking nucleophile, namely a water molecule or a hydroxyl group of (deoxy)ribose sugar. This interaction polarizes the O—H bond, lowering the nucleophile's pKa and facilitating its deprotonation to generate an activated nucleophilic species, either hydroxide or a 2′-alkoxide. The second metal M2 coordinates the oxygen atom of the leaving group, neutralizing the buildup of negative charge during the formation of the pentacovalent phosphorane-like transition state and stabilizes the departing leaving group (Fig. 1) [4].

This catalytic motif is widespread among protein enzymes that process nucleic acids. DNA polymerases, for example, utilize this mechanism to catalyze nucleotide addition during replication [43,44]. High-resolution crystal structures have captured the two Mg^{2+} ions in the active site, one interacting with the 3′-OH of the primer and the other with the triphosphate of the incoming (d)NTP [3]. Similarly, Ribonuclease H (RNase H), an enzyme that specifically degrades the RNA strand of RNA:DNA hybrids, employs a two-metal-ion active site formed by a conserved set of acidic residues (Asp and Glu) [6].

The discovery of ribozymes confirmed that RNA can independently fold to create active sites that recruit metal ions for catalysis [1,45,46]. The crystal structure of the group I self-splicing intron from *T. thermophila*, the first ribozyme for which a two-metal-ion mechanism was structurally verified, revealed two Mg^{2+} ions positioned exactly as predicted by the model, coordinating the guanosine nucleophile, the scissile phosphate, and the 3′-oxygen leaving group [8].

Moreover, the group II introns, thought to be the evolutionary ancestors of the spliceosome, were later shown to operate via the same two-metal-ion mechanism for both of their transesterification reactions needed for pre-mRNA splicing [9]. Arguably the most complex example of a two-Mg^{2+}-ion-dependent ribozyme is the spliceosome, where numerous cryo-EM determined structures have revealed a catalytic core formed by the U6 snRNA that positions two Mg^{2+} ions to catalyze both transesterification reactions underlying pre-mRNA splicing (i.e. the branching and exon ligation steps) [12,13,47].

While the core principles are highly conserved across different nucleic acid processing systems, mechanistic variations exist. Some enzymes utilize a third divalent metal ion to facilitate the reaction cycle. For example, in many DNA polymerases, a third Mg^{2+} ion transiently enters the active site to assist with the release of the pyrophosphate product [48]. However, the role of this additional metal ion remains controversial as different QM/MM studies assigned different roles in distinct systems. As an example, QM/MM calculations, in combination with the string method, of DNA polymerase η revealed that the electrostatic stabilization induced by the third Mg^{2+} ion lowers the free energy barrier of phosphoryl transfer reaction, and makes the reaction more thermodynamically favorable [49]. In this proposal, however, the identity of the base that activates the nucleophile remained uncertain. A water-mediated pathway, in which a Mg^{2+}-bound hydroxide serves as the base deprotonating the 3′-OH of the incoming nucleotide was also proposed [49]. However, this additional Mg^{2+} ion seems to inhibit the proton transfer from the 3′-OH to the leaving group as proposed in another QM/MM study where the third Mg^{2+} ion was instead suggested to aid the release of the pyrophosphate leaving group and to prevent pyrophosphorolysis, the reverse reaction of nucleotide addition [50]. Additionally, various QM/MM studies have shown that the identity of the metal ion (Mg^{2+} vs Na^{+}) shifts the relative equilibrium between nucleotide addition and pyrophosphorolysis reactions in polymerases [51,52].

Related protein metallohydrolases can also harbor auxiliary metal-binding sites near a dimetallic catalytic core. A representative example is the phosphodiesterase Rv0805 from *Mycobacterium tuberculosis*, whose activity is strongly modulated by binding of a calcium ion at a secondary pocket proximal to the active site [53]. Importantly, in this system Ca^{2+} appears not to directly participate in catalysis, but instead stabilizes a less active conformational state of the enzyme. While the mechanistic details differ from RNase systems, these observations illustrate that additional metal-binding sites adjacent to two-metal-ion catalytic centers can serve regulatory roles without contributing directly to the chemical step.

Consistent with this finding, multiple time-resolved X-ray

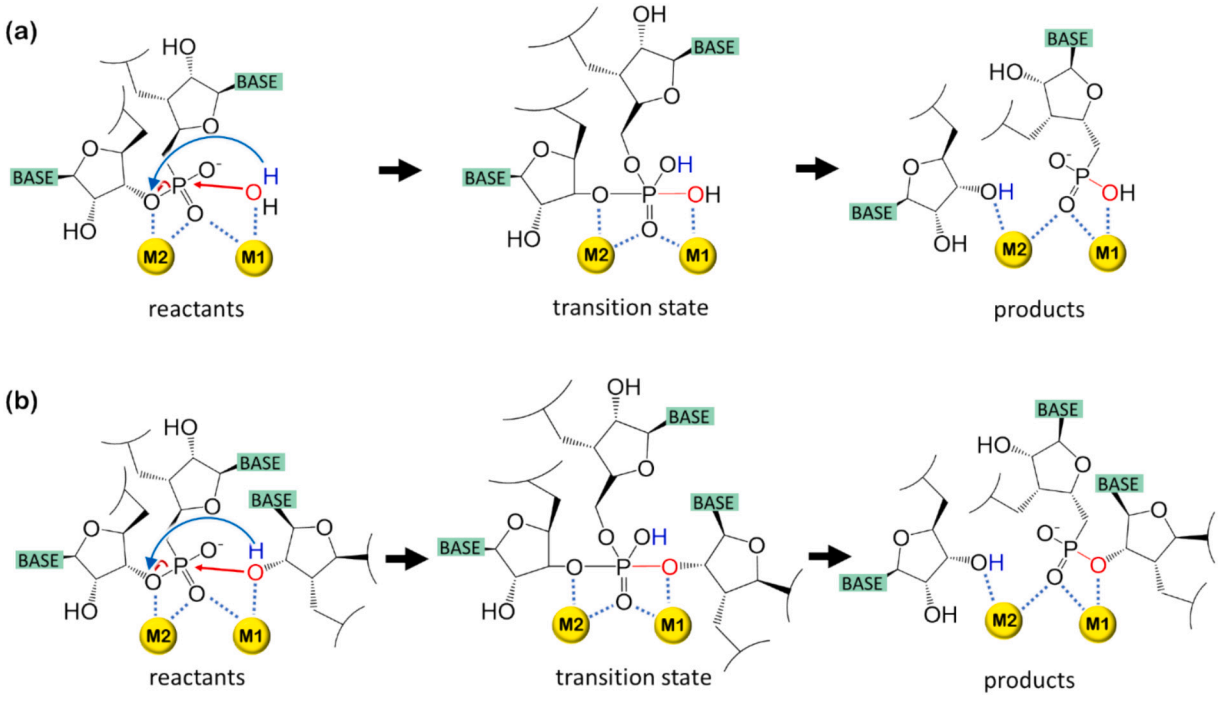

Fig. 1. Schematic representation of the Steitz and Steitz two-metal-ion catalytic mechanism. (a) Mechanism utilizing an activated water molecule (hydroxide) as the nucleophile. (b) Mechanism utilizing a ribose hydroxyl group (forming a 2′-alkoxide) as the nucleophile, based on first splicing step. In both pathways, the reaction proceeds through a pentacovalent phosphorane-like transition state. Metal ion M1 facilitates the deprotonation of the nucleophile, while M2 coordinates the oxygen of the leaving group to neutralize the developing negative charge.

crystallographic studies have revealed dynamic changes in metal-ion coordination at the active site during DNA cleavage [54] and DNA synthesis [48]. Metal ions bound at an enzyme's active site have finite lifetimes. If their residence time is shorter than or comparable to the enzyme's catalytic cycle, metal-ion dynamics can thus influence the rate and mechanism of enzymatic turnover. Indeed, single molecule FRET studies of λ-exonucleases showed that, while the two Mg^{2+} ions are stably bound and fully processive at high Mg^{2+} concentration, at a low concentration, occasional dissociation and slow re-coordination of Mg^{2+} (M1) result in pauses during processive degradation [55].

In contrast to DNA polymerases, QM/MM computational studies of RNA polymerases have predominantly focused on the canonical two-metal-ion mechanism and have not systematically investigated the role of a potential third metal ion in catalysis [56,57]. This disparity stems from several factors. First, the experimental evidence for a transient third metal ion in RNA polymerases remains less conclusive compared to DNA polymerases, where time-resolved X-ray crystallography has directly captured metal ion dynamics during the catalytic cycle [44]. Indeed, RNA polymerase II, being a significantly larger and more complex 12-subunit enzyme compared to the relatively compact single-chain DNA polymerases, presents greater challenges for obtaining high-resolution structures of catalytic intermediates that would reveal transient metal binding events. The lack of definitive structural snapshots showing a third metal ion in RNA polymerase active sites during nucleotide addition has thus limited computational investigations into whether such a mechanism operates in transcription, leaving this as an open question for future time-resolved crystallographic and computational studies.

Conversely, the growing number of experimentally determined (ribo)enzyme structures reveals that the canonical two-metal-ion motif can be supplemented by additional ions. This is apparent in ribozymes, namely the group II intron, in which the two-Mg^{2+}-motif is flanked by K^+ ions, and the overall structure is decorated by many Mg^{2+} and K^+ ions [16]. This phenomenon may be more common than previously thought, particularly in complex RNP machines. Variations in metal-ion composition and dynamics highlight the flexibility of the two-metal-ion framework, which can be elaborated with additional components to meet the specific energetic and mechanistic demands of a given catalytic cycle [2,23,58,59].

4. Monovalent ions: Emerging players

In RNA biology, the roles of monovalent cations like K^+, the most abundant cellular cation, and Na^+ ions were for decades primarily attributed to non-specific electrostatic screening of the negatively charged phosphate backbone, which is essential for RNA folding into compact tertiary structures [60,61]. While specific binding sites for monovalent ions were identified in structural pockets of some ribozymes, such as the hammerhead [62] and HDV ribozymes [63], and group II introns [16], they were generally considered to play a structural rather than a direct catalytic role. However, a re-examination of high-resolution ribosome structures [22,64], by applying rigorous stereochemical criteria, revealed a significant number of electron densities previously assigned as Mg^{2+} were in fact better modeled as K^+. This work revealed that K^+ ions are not just diffusely associated with the RNA surface, but occupy specific, well-defined pockets where they establish direct coordination with RNA functional groups, often outnumbering tightly bound Mg^{2+} ions. This fundamental insight prompts the re-evaluation of ion assignments across many RNA structures [22].

The most compelling evidence for a direct catalytic role for a monovalent ion comes from the structural study of the spliceosome, captured just after the first catalytic step. Here, a strong, unassigned electron density in the heart of the active site, located approximately 5 Å from the two catalytic Mg^{2+} ions was discovered [20]. This density was assigned as a K^+ ion, coordinated by conserved nucleotides of the U6 and U2 snRNAs. Critically, this K^+ binding site is occluded by the protein factor Prp8 in the pre-catalytic state, indicating that K^+ binding is coupled to the activation of the spliceosome (Fig. 2a and b). This K^+ ion is fully conserved also in the group II intron ribozyme, the evolutionary ancestor of the spliceosome. Functional experiments confirmed its importance, as replacement of monovalent metal ions significantly impaired the rate and fidelity of the branching reaction [20].

As such, the specific roles of these catalytic monovalent ions might be multifaceted, extending from large-scale assembly to possible direct participation in the catalytic processes. Their binding or release can be coupled to major conformational rearrangements, serving as a checkpoint during the assembly and activation of the catalytic machinery, as seen in the spliceosome [23,67]. Furthermore, by binding in specific pockets, monovalent ions can act as molecular staples, locking the flexible RNA components of the active site into a catalytically competent conformation [68]. Recent high-resolution analysis of the yeast P complex reveals that this K^+ ion is preserved within the active site even after exon ligation. In this post-catalytic state, the ion appears to stabilize the complex by bridging the base pair between the 5′ (+1G) and 3′ (−1G) splice sites (Fig. 2c) [66].

Additional evidence of metal ions transiently occupying the catalytic site comes from an RNase H study [65], in which time-resolved crystallography revealed a dynamic “cation trafficking” mechanism essential for catalysis. By capturing reaction intermediates, it was shown that the two canonical Mg^{2+} ions were insufficient for hydrolysis. Instead, the reaction required the transient recruitment of additional ions, namely a third Mg^{2+} and two additional K^+ ions. A first K^+ ion was observed to initially occupy the active site (Fig. 2d), but to be soon replaced by the third Mg^{2+} ion, which correctly positions the nucleophilic water to herald the attack. Interestingly, a second K^+ ion was also captured coordinating the scissile phosphate, thereby stabilizing the substrate alignment and product formation.

These findings collectively demonstrate that monovalent ions are most likely not just passive spectators, but are active players in the catalytic cycle of many RNA processing (ribo)enzymes. Future structural, functional and computational studies should therefore explicitly consider the identity and role of monovalent cations in the active site.

5. Computational insights into combined ionic effects in ribozymes

The dynamic and complex nature of multi-ion catalytic sites presents significant challenges for experimental characterization alone. Static experimentally determined structures provide invaluable snapshots, but they cannot capture the conformational dynamics, transient intermediates, and proton transfer events that define the reaction pathway. While some reaction mechanisms can be determined experimentally at atomic-level detail using time-resolved X-ray crystallography [65] or cryo-EM, these studies are rare and are still challenging for large (ribo)zyme systems. Computational simulations, particularly all-atom MD and hybrid QM/MM methods [26], have become essential for bridging this gap and providing a motion-picture view of catalytic processes [2].

MD simulations, run over microsecond timescales, can capture slower processes such as ion trafficking and minor conformational changes. These simulations have shown that ions are not static components but can dynamically enter and leave the active site region during the catalytic cycle. In classical MD simulations, additional cations, either monovalent ions or a transient third Mg^{2+} ion, can be observed to diffuse from the bulk solvent into auxiliary binding pockets, which modulate active-site geometry across different enzyme families [59], thus influencing substrate positioning and product release [69,70]. Collectively, these classical MD studies emphasize that multi-ion architectures in nucleic-acid processing enzymes are inherently dynamic, with both divalent and monovalent ions continuously rearranging around the active site to support different stages of the catalytic cycle.

On the other hand, QM/MM MD simulations, which treat the

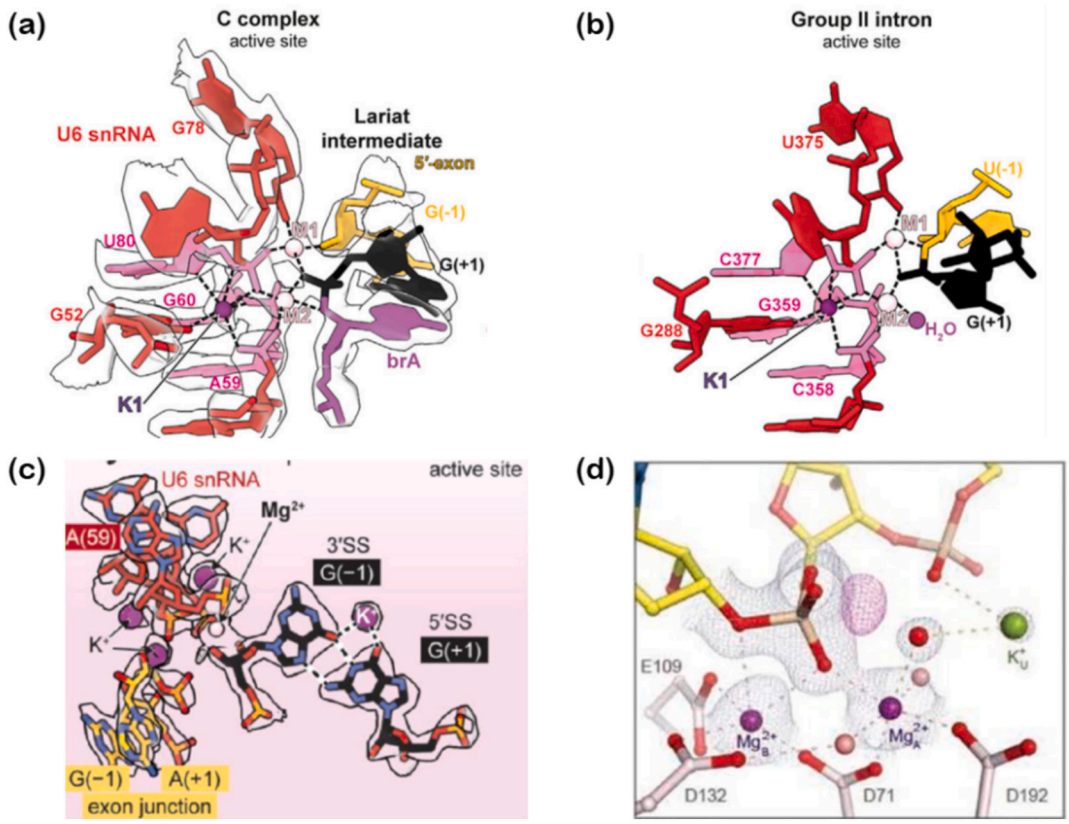

Fig. 2. Experimentally determined monovalent K^+ ion at the two-metal-ion catalytic sites. Close view of (a) the spliceosome C complex active site containing the structural K^+ ion (labeled K1, purple sphere), positioned within the catalytic core, coordinated by conserved nucleotides of the U6 snRNA (red) and located approximately 5 Å from the two catalytic Mg^{2+} ions (M1 and M2); (b) the active site of a group II intron ribozyme, the evolutionary ancestor of the spliceosome. A homologous K^+ ion (K1) is fully conserved in this structure, occupying a specific pocket and coordinating with RNA functional groups similarly to the spliceosome; (c) the active site of the yeast spliceosome P complex in the post-catalytic state. The K^+ ion is preserved after exon ligation, where it stabilizes the complex by bridging the base pair between the 5′-exon (G + 1) and the 3′-splice site (G-1) at the exon junction; (d) the active site of RNase H1 in time-resolved crystallography at the start of reaction (t = 80 s), with K^+_U ion (green sphere) initially coordinating nucleophilic water. Adapted and reprinted with permission from references [20, 65, 66]. (For interpretation of the references to colour in this figure legend, the reader is referred to the web version of this article.)

reactive core with high-level QM methods and the surrounding enzyme and solvent with classical MM force fields, have been instrumental in validating and refining the chemical details of the two-metal-ion mechanism. Initial QM/MM-based studies of RNA processing were performed on RNase H. Complemented by enhanced sampling methods to explore the free energy surface associated with the reactive events they revealed an associative S_N2 pathway, with bond formation preceding bond breakage, and quantified the activation free energy barrier in good agreement with experimental kinetics [26,71,72]. While the S_N2 pathway was generally confirmed in other studies [73–76], the proton transfer events underlying nucleophilic water activation and leaving group stabilization remained controversial. Indeed, the phosphate cleavage and transfer are inherently coupled to proton transfer events, in which the attacking nucleophile must be activated (deprotonated), while the leaving group requires protonation to complete the reaction. Enzymes and ribozymes must deprotonate the incoming nucleophile, such as the hydrolytic water or hydroxyl groups of the nucleotide's ribose, which are initially bound in their neutral form rather than as reactive hydroxide or alkoxy ions. Deprotonation most often occurs concurrently with nucleophilic substitution [77] and is facilitated by active-site charged residues and metal ions, especially Mg^{2+}, which modulate the local pKa values. These mechanistic principles apply broadly across enzymes, and numerous experimental studies show that proton transfer is often part of the rate-limiting step [78].

A central challenge is determining the precise location of protons during reactions. Proton transfer is an inherent component of chemical mechanisms, and enzymes have evolved catalytic strategies to optimize these events. However, proton positions are rarely observed experimentally, even in stable reactant or product complexes. Hybrid QM/MM approaches enable us to investigate proton transfer events alongside the electronic density changes that drive bond breaking and formation, not only at local minima but also along the entire reaction coordinate, including transition-state structures. Furthermore, the number, type, and positioning of metal ions strongly affect proton transfer events, the catalytic mechanism, and the associated free energy profile [58,79]. QM/MM MD methods can also rationalize the effects of ion substitutions [23]. For example, simulations of RNase H with inhibitory Ca^{2+} instead of Mg^{2+} revealed that the larger Ca^{2+} ion subtly distorts the active site geometry, preventing the system from reaching the optimal transition state conformation [80]. Conversely, substituting Mg^{2+} with Mn^{2+} in polymerases has been shown to enhance catalytic efficiency [75].

A series of crystal structures of a reduced group II intron construct, corresponding to several steps of the splicing process, revealed that reactants are activated by a heteronuclear four-metal-ion center containing a two-Mg^{2+}-ion cluster and monovalent cations. In particular, the two magnesium ions (M1 and M2) and the K1 ion are coordinated by specific ligands, namely the O^{Rp} oxygen of the scissile phosphate and the O^{Sp} oxygen of C377, respectively [16].

This heteronuclear ion cluster is suggested to be a unique attribute of RNA enzymes and constitutes an essential cofactor for group II intron catalysis. Indeed, functional studies have demonstrated that substituting K^+ with Na^+ impairs splicing, an effect largely attributed to the role of K^+ in supporting the intron's functional structure. This reduced group II intron construct, featuring a solvent-exposed active site, allowed the

first splicing step to follow a hydrolytic path. A computational study aiming to investigate the cleavage of the 5′-exon from this ribozyme combined thermodynamic integration with hybrid QM/MM MD simulations using the BLYP/B3LYP exchange correlation functionals and the Amber ff14SB and χOL3 force fields for the QM and MM region, respectively. Remarkably, this study revealed a new RNA-specific dissociative mechanism, in which the bulk water received the proton of the nucleophile, after the water nucleophilic attack [41]. This was likely due to the solvent accessibility of the active site.

Despite the evolutionary link between group II introns and the spliceosome, initial cryo-EM structures of the latter did not fully resolve the active site's ion composition. Consequently, early static QM/MM studies of the first splicing step considered only two Mg^{2+} ions. This approach yielded a free energy barrier of ~21.5 kcal/mol and a reaction free energy of ~1.8 kcal/mol, predicting a dissociative pathway, in which bond breaking preceded bond formation without forming any intermediate [81]. However, the catalytic role of the K^+ ion was later confirmed for the spliceosome's branching reaction [20]. In addition to cryo-EM studies locating a K^+ ion at the K1 position, ion replacement experiments showed that K^+ increased forward splicing efficiency. This hypothesis was supported by QM/MM MD simulations, combined with thermodynamic integration, using the DFT-BLYP level of theory and Amber ff14SB and χOL3 force fields for the QM and MM part, respectively. These calculations showed that the K^+ ion rigidifies the RNA scaffold and helps facilitate the branching reaction [23]. Furthermore, with the inclusion of K^+, the reaction was found to follow an associative mechanism as originally predicted by Steitz and Steitz for two-Mg^{2+}-ion aided catalysis.

The obtained free energy profile, when K^+ occupies the K1 binding site, exhibited two transition states separated by a shallow intermediate. The Helmholtz activation free energy barrier ($\Delta F^{\ddagger}$) to reach the intermediate state from the reactant state was significantly larger ($\Delta F^{\ddagger} = 13.6 \pm 0.4$ kcal/mol) than that required to arrive from the intermediate to the product state ($\Delta F^{\ddagger} = \sim 2$ kcal/mol), making the first transition the rate-limiting step. The reaction free energy was negative ($\Delta F = -4.2 \pm 0.9$ kcal/mol), indicating intron lariat formation was energetically favorable.

As such, the K^+ ion lowers the activation free energy barrier for branching reaction and stabilizes the product state, thereby promoting forward splicing. Specifically, in the presence of K^+, the nucleophilic 2′-OH forms a stable hydrogen bond with G(+1)-O^{Sp} as it approaches the scissile phosphate prior to the first transition state. The proton is then transferred from the nucleophile (branch point adenosine (BPA)-O2′) to G(+1)-O^{Sp}, facilitating the formation of the BPA-O2′–G(+1)-P bond. The critical role of this proton transfer to G(+1)-O^{Sp} is consistent with findings from sulfur substitution experiments [82]. In the intermediate state, a hydrogen bond forms between the proton on G(+1)-O^{Sp} and a water molecule that enters the active site from the bulk solvent. The subsequent cleavage of the 5′-exon–intron link (the G(−1)-O3′–G(+1)-P bond) occurs via an almost barrierless transition state. During this step, the proton on G(+1)-O^{Sp} rotates away from the water molecule and is transferred to the G(−1)-O3′ leaving group. Throughout the reaction, the K^+ ion remains stably coordinated in its binding site, maintaining a constant distance from both M1 and M2.

Since functional studies indicated that Li^+ ions decreased overall splicing efficiency [20], the reaction mechanism was also investigated by replacing the K^+ with Li^+ ion in QM/MM MD simulations [23]. Even during the unbiased simulations, the Li^+ ion failed to maintain a stable coordination sphere at the K1 site and was instead continuously shuttling between coordinating partners. This instability likely arose from the notable differences in ionic radius and coordination preferences between Li^+ and K^+. Furthermore, the presence of K^+ was found to lower the activation free energy barrier by several kcal/mol compared to systems containing Li^+ or lacking a monovalent ion entirely [23,81]. Indeed, although the overall reaction mechanism remained unchanged in the presence of Li^+ the $\Delta F^{\ddagger}$ for the rate-limiting step increased to 16.2 ± 0.5 kcal/mol and the ΔF decreased to −2.3 ± 0.9 kcal/mol, driven by reduced stability of the product state, in agreement with experimental observations showing increased reversal of the reaction [21].

A comparison of distances between relevant atoms in the active site revealed key differences as the reaction approached the first transition state. Namely, the average distance between the 2'-OH proton of BPA and G(+1)-O^{Sp} was larger and displayed higher fluctuations in the presence of Li^+ in the active site, indicating a less stable hydrogen bond. This hydrogen bond (hb1 in Fig. 3) preceded and facilitated the proton transfer from the nucleophilic 2'-OH of BPA to the scissile phosphate, crucial for BPA-O2'–G(+1)-P bond formation. Additionally, in the second transition state, the hydroxyl group of the scissile phosphate formed a hydrogen bond with G(−1)-O2' instead of a water molecule (hb2 in Fig. 3), as observed in simulations with K^+ in the active site, explaining the larger second activation free energy barrier (~3.2 kcal/mol). Analysis of hydrogen-bonding frequencies showed that both hb1 and hb2 were established more often when K^+ occupied the monovalent ion site. These differences likely stemmed from the less stable binding of Li^+, which increases the flexibility of the catalytic site. Importantly, these results show that it is not only the presence of a monovalent ion that matters, but the specific identity of the ion itself, which critically tunes the free energy barrier, with K^+ enabling markedly more favorable catalysis than the Li^+ ion (Fig. 3) [23].

The functional dependence on specific monovalent cations extends to the RNase MRP [83]. This RNA-based machinery cleaves the 5′-end of pre-rRNA at the A3 site within internal transcribed spacer 1 (ITS1) using a water molecule as the attacking nucleophile. A recent classical and QM (BLYP)/MM (Amber ff14SB) MD simulations in combination with thermodynamic integration elucidated the catalytic contributions of different metal cofactors explicitly introduced into the active site [58]. Although cryo-EM structures initially identified a third Mg^{2+} ion within the catalytic core [15], the QM/MM MD simulations demonstrated that this divalent cation actually functions as an inhibitor, stabilizing the reactant state and impeding the necessary proton transfer [58]. Specifically, the presence of the three Mg^{2+} ions did not allow the reaction to occur even when $\Delta F^{\ddagger}$ overcome a barrier larger than 40 kcal/mol, indicating that for the reaction to proceed, this third Mg^{2+} must be removed. When the third metal ion was removed, monovalent ions present in the ionic buffer diffused near the active site. However, when MD simulations were performed in NaCl solution and a Na^+ ion diffused close to the active site, the catalytic process was still disfavored with $\Delta F^{\ddagger} > 35$ kcal/mol. The simulation outcomes changed when performed in KCl solution. Here, a K^+ ion is diffused near nucleophile, the reaction finally occurred via associative mechanism and the free energy barrier was compatible with an effective catalytic process ($\Delta F^{\ddagger} = 18.5 \pm 1.3$ kcal/mol) (Fig. 4). Indeed, the experimental catalytic rate of 0.25 min^{-1} corresponding to a Gibbs free-energy barrier $\Delta G^{\ddagger}$ of 20.7 kcal/mol, was in good agreement with the computed $\Delta F^{\ddagger}$ value. The MRP machinery catalyzed rRNA processing via the following steps: (i) a proton was initially shuttled from the nucleophilic water to the O^{Sp} atom of the scissile phosphate through a supporting water molecule. This synchronous double proton transfer occurred just before the first transition state was reached. (ii) Once the nucleophilic water was deprotonated to a hydroxide ion, it performed the nucleophilic attack on the P atom of the scissile phosphate, forming a metastable phosphorane intermediate, which was cooperatively stabilized by both M1 and M2 Mg^{2+} ions. (iii) A second, almost barrierless transition state was overcome for dissociating the leaving group, and (iv) this was eventually followed by a direct proton transfer from the protonated O^{Sp} oxygen of the scissile phosphate to the O3′ of the leaving group, thus leading to product formation (Fig. 4).

Much like the findings in the spliceosome, the specific identity of the monovalent ion was important, as Na^+ failed to meet the strict geometrical requirements of the pocket, whereas the K^+ ion was uniquely able to coordinate the phosphate backbone and orchestrate a

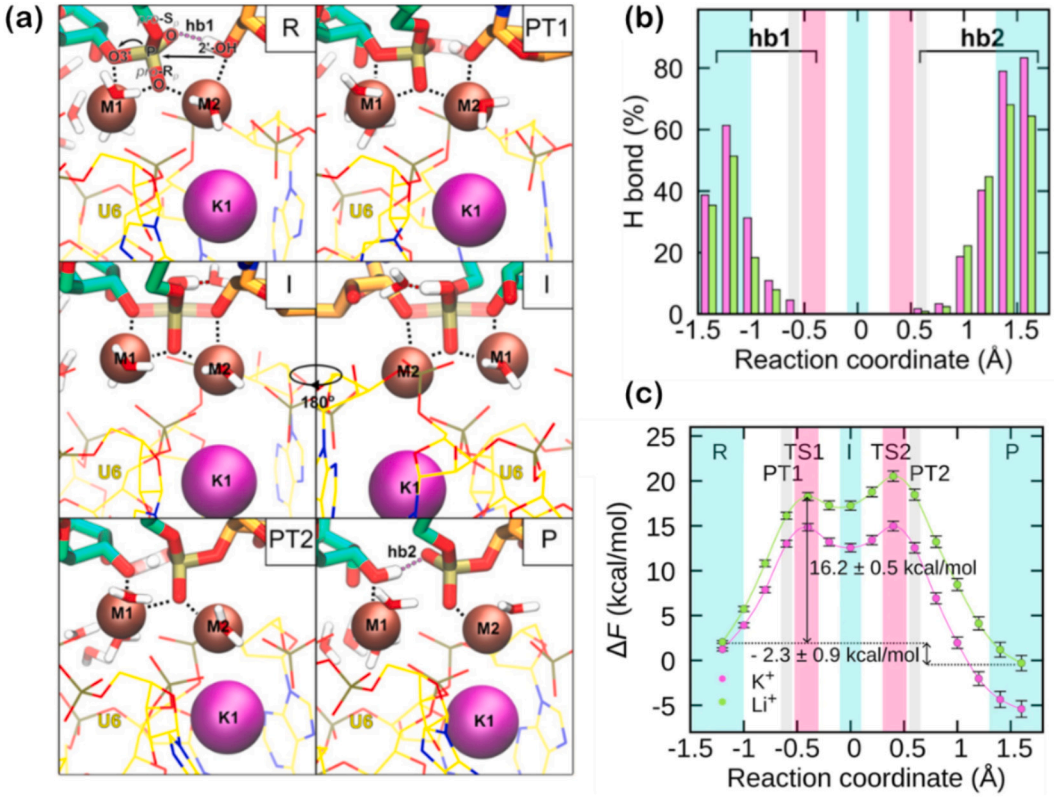

Fig. 3. Reaction mechanism of the spliceosome branching step investigated by QM/MM MD simulations. (a) Representative snapshots of the reactant (R), first proton transfer (PT1), intermediate (I), second proton transfer (PT2), and product (P) states. The active site shows the coordination of the Mg^{2+} ions (M1, M2), the monovalent potassium ion at the K1 site, and the hydrogen bonding network involving the scissile phosphate and water molecules. (b) Frequency (percentage) of key hydrogen bonds observed along the reaction coordinate. The hb1 region corresponds to the hydrogen bond between the nucleophilic 2'-OH of the branch point adenosine and the scissile phosphate oxygen (G(+1) – O^{Sp}), while hb2 corresponds to the hydrogen bond involving the protonated scissile phosphate and the leaving group. Magenta and light green bars report values obtained for the system containing K^+ and Li^+ ions, respectively. (c) Helmholtz free energy profiles (ΔF [kcal/mol]) calculated for the branching reaction in the presence of K^+ (magenta) and Li^+ (light green). The profile highlights the two transition states (TS1, TS2) separated by an intermediate (I), along with the specific proton transfer events (PT1, PT2). The activation free energy barrier and reaction free energy values are indicated for the K^+ pathway. Adapted and reprinted with permission from reference [23]. (For interpretation of the references to colour in this figure legend, the reader is referred to the web version of this article.)

precise hydrogen-bonding network. Again, in RNase MRP, the K^+ ion optimally oriented the nucleophilic water and a secondary supporting water, thereby lowering the free energy barrier for the essential water-mediated proton transfer from the nucleophile to the O^{Sp} oxygen of the scissile phosphate. A detailed analysis of the two catalytically-relevant water molecules in the active site during unbiased QM/MM MD simulations of the reactant state revealed that, due to different size and coordination preferences, the two ions occupy a different position with respect to the phosphate backbone of A1 and C2, with K^+ positioned closer to the scissile phosphate (Fig. 4). Most importantly, an analysis of the hydrogen bonding between the proton of the nucleophilic water (wat_{nuc}) and the oxygen of the supporting water (wat_s) (O_{nuc} – $H_{watnuc}\cdots O_{watS}$), as well as between the proton of the supporting water and the O^{Sp} oxygen of the scissile phosphate (O_{watS} – $H_{watS}\cdots O^{sp}$) along the reaction coordinate revealed that the simultaneous formation of $O_{watS}\cdots H_{watnuc}$ and $H_{watS}\cdots O^{Sp}$ hydrogen bonds was more frequent in the presence of K^+ ion rather than the Na^+ ion. As a result, only K^+ ion allowed the wat_{nuc} and wat_S molecules to optimally align for the double proton transfer from the wat_{nuc} to the scissile phosphate via the supporting wat_S molecule (Fig. 5).

Thus, the RNase MRP machinery relies not merely on the static presence of ions captured in experimental structural studies, but rather on a regulated exchange of additional ions. The inhibitory Mg^{2+} ensures proper substrate conformation before yielding to the catalytic K^+, highlighting a sophisticated role for second-shell metal ions in switching on and off the catalysis and fine tuning the energetics of phosphodiester bond cleavage [58].

To further support the finding of the spliceosome and RNase MRP, the role of a third metal ion in ribozyme cleavage was already proposed in 1999 for group I intron ribozyme. Here, functional studies suggested that a third metal ion interaction could help activating the nucleophile and to properly position the reactive phosphoryl group with respect to the nucleophile, thereby accelerating the transesterification reaction [84]. In summary, the **presence, position** and the **identity** of monovalent ions appear to act as fine regulators of catalytic efficiency in RNA processing machineries.

6. Mechanism-specific considerations

While the multi-ion framework of the catalytic site is a recurring theme, the precise chemical mechanism beyond Steitz and Steitz's general two-Mg^{2+}-ion scheme [4] appears to be system specific. However, the molecular features discriminating between the possible paths are unclear [71–74,85]. The knowledge gained from computational studies nevertheless allows us to formulate possible general principles. A primary determinant of the mechanistic pathways in RNA metabolism is the identity of the nucleophile, which is either a water molecule in hydrolysis reactions, or a nucleic acid-borne 2′- or 3′-hydroxyl group of (deoxy)ribose in transesterification reactions. From the many studies of the catalytic mechanism of nucleic-acid processing (ribo)enzymes it clearly emerges that when RNA is metabolized via a hydrolytic mechanism, the proton transfer accompanying phosphodiester bond cleavage

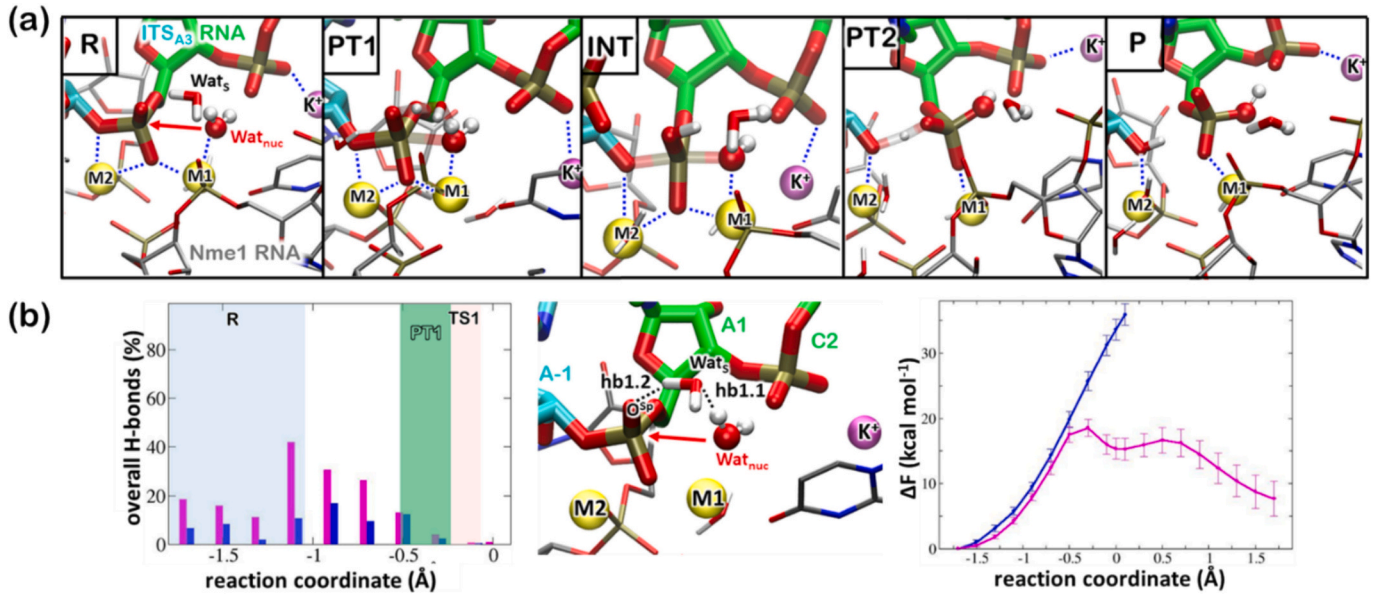

Fig. 4. Reaction mechanism of MRP-catalyzed rRNA processing revealed by QM/MM MD simulations. (a) Snapshots of the reactant state (R), first proton transfer (PT1) event, intermediate state (INT), second proton transfer (PT2) and product (P) state of pre-rRNA processing reaction. Wat_{nuc} denotes nucleophilic water and Wat_S supporting water. (b) Frequency of double hydrogen bonding simultaneously occurring between the hydrogen of the nucleophilic water and the oxygen of supporting water (hb1.1) and between the hydrogen atom of supporting water and the O^{Sp} oxygen of the scissile phosphate (hb1.2) as a function of the reaction coordinate (TI windows: −1.5, −0.7, −0.5, −0.3). The magenta and blue bars report values obtained for the system containing a K^+ ion and a Na^+ ion in the catalytic site, respectively. Middle panel shows close up of the active site with the distances hb1.1 and hb1.2 and angles α and β, which define the first and second hydrogen bond. Right panel depicts Helmholtz free energy profile (ΔF [kcal/mol]) calculated from the thermodynamic integration for K^+ (magenta) and Na^+ (blue) systems. Standard deviation of the ΔF at each point of the reaction coordinate is shown in bars. Adapted and reprinted with permission from reference [58]. (For interpretation of the references to colour in this figure legend, the reader is referred to the web version of this article.)

is water-assisted [14,21,41,58,71]. Namely, the proton of the nucleophile is first received by a water molecule and then is typically shuttled to the scissile phosphate [14,21,41,58,71], or, sometimes, to a nearby phosphate [72]. This highly depends on the specific geometry and the solvent exposure of the active site. Conversely, when the transesterification reaction occurs with the (deoxy)ribose 2′- or 3′-hydroxyl group acting as the nucleophile, the proton is transferred directly from the nucleophile to the scissile phosphate [23,81,86]. The likely explanation for this phenomenon is the positional stability and orientation of the ribose hydroxyl. Compared to a water molecule, the ribose moiety is more rigid, and geometrically constrained, allowing the hydroxyl group to maintain a constant hydrogen bond with the O^{Sp} oxygen of the scissile phosphate at the optimal angle [23,86]. In contrast, a water molecule, although being coordinated to a Mg^{2+} ion (M1), is more mobile, and tends to form transient hydrogen bonds with various nearby residues and/or to the solvent water molecules (Fig. 6) [14,41,58,71,72].

As additional general considerations we observed that in systems where a proton is transferred from the nucleophile to the scissile phosphate and subsequently to the leaving group, the free energy profile typically entails two transition states separated by a pentacovalent phosphorane-like intermediate. The first transition state corresponds to the complete proton transfer to the scissile phosphate, while the second corresponds to the deprotonation of the phosphate and the subsequent proton transfer to the leaving group [23,58,71,86]. Conversely, when the proton is not transferred via the scissile phosphate, the free energy profile exhibits only a single transition state with no intermediates [41,74].

Regarding the progression of the concerted S_N2-like mechanism, QM/MM studies of nucleic acid catalysts predominantly support an associative pathway. In this scenario, bond formation is more advanced than bond breaking at the transition state [23,58,71,74]. Less frequently, a dissociative mechanism, where bond breakage is more advanced than bond formation, is observed [41,47]. It remains unclear whether this discrepancy arises from inherent structural system subtleties or from methodological factors, such as the choice of starting structure. However, it appears that studies derived from more stable catalytic sites with well-resolved components favor the associative mechanism.

7. Future directions

A deep mechanistic understanding of the extended two-metal-ion architecture in RNA processing enzymes could have implications for biotechnology and medicine, particularly in the rational design of RNA-based therapeutics and gene-editing tools. While the recent resolution revolution in cryo-EM has provided unprecedented views of these large ribonucleoprotein complexes, these structures often represent static minima on a complex energy landscape, frequently failing to resolve the highly mobile solvent and ionic species critical for function. A major challenge for the field is therefore to transition from static structural snapshots to a dynamic multidimensional mapping of the catalytic cycles. This will require a tighter integration of time-resolved structural biology methods, such as X-ray crystallography and time-resolved cryo-EM, with advanced computational modeling. Specifically, the ambiguity of electron density maps regarding positioning and folding of nucleic acids as well as the identity of lighter monovalent species versus water molecules necessitates the development of automated refinement tools. Emerging approaches based on extensive all-atom simulations [87], leveraging deep learning [88–90] and rigorous stereochemical validation [91] are beginning to address this challenge, offering robust strategies to distinguish between potassium, sodium, magnesium, and solvent densities based on coordination geometry and local electrostatic environments. In particular, recent machine-learning approaches trained on high-resolution structural data have begun to assist in the identification and discrimination of monovalent and divalent ions from water molecules in RNA structures, using coordination geometry, local electrostatics, and stereochemical constraints. While these tools already improve ion assignment in cryo-EM and crystallographic maps, their

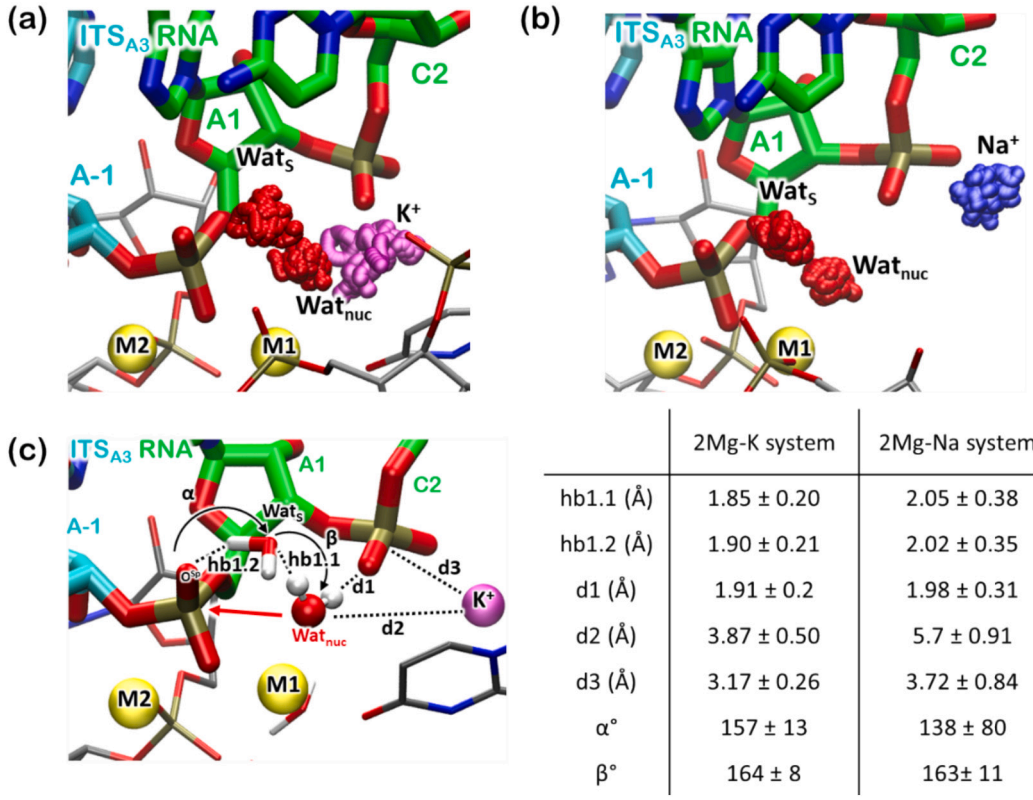

	2Mg-K system	2Mg-Na systems
hb1.1 (Å)	1.85 ± 0.20	2.05 ± 0.38
hb1.2 (Å)	1.90 ± 0.21	2.02 ± 0.35
d1 (Å)	1.91 ± 0.2	1.98 ± 0.31
d2 (Å)	3.87 ± 0.50	5.7 ± 0.91
d3 (Å)	3.17 ± 0.26	3.72 ± 0.84
α°	157 ± 13	138 ± 80
β°	164 ± 8	163± 11

Fig. 5. Close up view of the RNase MRP catalytic site. Spatial density, illustrating the occupancy of the nucleophilic (Wat_{nuc}) and supporting (Wa_tS) water molecules for MRP catalytic site during QM/MM MD simulations of the reactant state, is shown as red surfaces, for (a) the K^+ ion system (2 Mg-K model) featuring a flanking potassium ion (magenta surface) and (b) the Na^+ ion system (2 Mg-Na model) with a sodium ion (blue surface). (c) Close-up view of the active site (left) with defined geometric parameters (bonds and angles) in yellow. The adjacent table (right) lists the mean values and standard deviations for distances hb1.1, hb1.2, d1-d3 and angle α and β across both the 2 Mg-K and 2 Mg-Na systems, derived from plain QM/MM MD simulations. Adapted and reprinted with permission from reference [58]. (For interpretation of the references to colour in this figure legend, the reader is referred to the web version of this article.)

performance remains limited in highly dynamic, metal-dense catalytic cores, underscoring the need for larger curated training sets and tighter integration with physics-based simulations [88–91].

On the computational front, the accurate simulation of these multi-ion systems faces significant hurdles that must be addressed to fully decode the second-shell regulatory mechanisms. Standard fixed-charge force fields often struggle to capture the complex polarization effects and charge transfer events induced by high-density metal clusters within the RNA core [92]. Consequently, the broader adoption and refinement of polarizable force fields can aid in correctly predicting the competitive binding and subtle structural modulation exerted by auxiliary monovalent ions [93–95].

The emerging machine learning potentials represent a transformative frontier, promising to bridge the gap between the accuracy of quantum mechanics and the sampling capability of molecular mechanics. By training neural network potentials on high-level quantum mechanical data, it could become possible to simulate entire catalytic cycles, including proton transfer events and dynamic ion rearrangements, with ab initio accuracy at a fraction of the computational cost [96–98]. This approach could resolve the lingering controversies regarding associative versus dissociative pathways by allowing for statistically significant sampling of reactive trajectories, rather than relying on minimum energy paths. Such methods would enable the construction of comprehensive free energy landscapes that account for the entropic contributions of the mobile ion cloud and the surrounding solvent, providing a more rigorous thermodynamic basis for the observed catalytic rates.

Notably, despite their promise, fully polarizable force fields and machine-learning potentials have not yet been applied to phosphodiester cleavage reactions in ribozymes or RNA-based machineries, largely due to the lack of transferable models for metal-rich RNA active sites.

Beyond the fundamental mechanistic insights, the recognition that monovalent ion binding pockets are structurally distinct and highly specific to each enzymatic system offers a novel pharmacological opportunity. Unlike the universally conserved two-metal-ion core, which is difficult to target selectively across different polymerases and nucleases, the diverse landscape of second-shell auxiliary sites presents a unique structural fingerprint for drug discovery. Future efforts should focus on mapping these sites to identify cryptic pockets that are only transiently formed during specific stages of the reaction coordinate [99–101]. Exploiting these sites with small molecules or antisense oligonucleotides that displace catalytic monovalent ions or stabilize inhibitory conformations could lead to a new generation of highly specific modulators for nucleic acid processing machineries.

Although the two-Mg^{2+} catalytic core is conserved, auxiliary monovalent-ion pockets exhibit system-specific structural and dynamical fingerprints across RNA machineries. In the spliceosome, the K^+ site is a deeply embedded, conformationally gated RNA pocket that rigidifies the active site and indirectly supports proton transfer during transesterification, whereas in RNase MRP the K^+ ion occupies a more solvent-exposed, dynamically exchanged site that primarily organizes catalytic waters for hydrolytic cleavage, enabling highly specific modulation.

Ultimately, the field is moving toward a holistic description of RNA catalysis where the protein-RNA scaffold, the solvent, and the multi-metal-ion atmosphere are treated as an inseparable functional unit. The integration of high-resolution structural data with multiscale

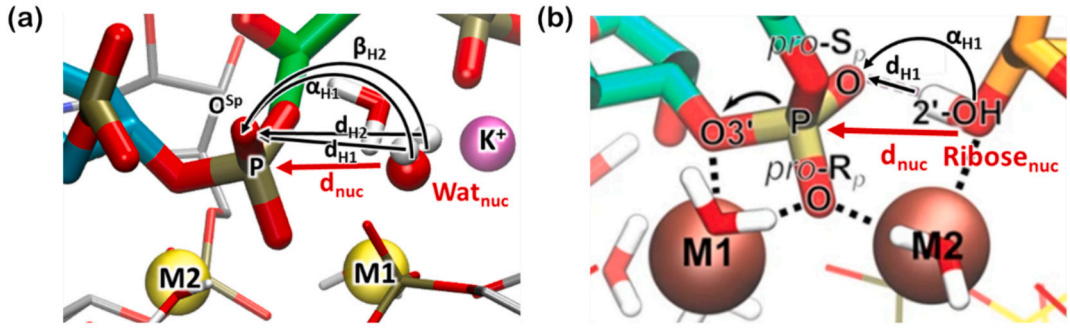

(c)

distance/ angle	water nucleophile (MRP system)	ribose nucleophile (spliceosome)
d_{nuc} (Å)	3.44 ± 0.29	3.14 ± 0.15
d_{H1} (Å)	3.40 ± 0.40	2.09 ± 0.45
d_{H2} (Å)	4.21 ± 0.37	-
α_{H1} (°)	107 ± 14	145 ± 27
β_{H2} (°)	59 ± 15	-

Fig. 6. Close up view of the catalytic sites depicting key distances (d_{nuc} = O_{nuc} - P; d_{H1} = H1 - O^{Sp}; d_{H2} = H2 - O^{Sp}) and angles (α_{H1} = O_{nuc} - H1 - O^{Sp}; β_{H2} = O_{nuc} - H2 - O^{Sp}) of nucleophile and nucleophile proton(s) to scissile phosphate P and O^{Sp} (labeled as pro-S_p in the spliceosome system). (a) Representation of the active site of RNase MRP showing the key geometric parameters (distances and angles) defining the orientation of the water nucleophile (Wat_{nuc}) relative to the scissile phosphate. (b) Representation of the active site of the spliceosome before the branching reaction showing the key geometric parameters (distances and angles) defining the orientation of the ribose 2'-OH nucleophile ($Ribose_{nuc}$) relative to the scissile phosphate. (c) Table comparing the computed average distances and angles from unbiased QM/MM MD simulations, together with their standard deviations, for a water nucleophile (RNase MRP) versus a ribose nucleophile (spliceosome). Adapted and reprinted with permission from reference [23, 58].

simulations will likely uncover that many apparent background electrolytes are in fact evolved, functional elements of the enzymatic machinery. Deciphering this ionic code will not only refine the current understanding of basic ribozyme chemistry, but also provide the blueprint for engineering novel gene-editing enzymes with tunable activities and specificities, moving beyond simple steric blockers to sophisticated tuners of enzymatic chemistry.

8. Conclusion and perspective

The two-metal-ion mechanism, first proposed over three decades ago, remains a central and unifying principle in the catalysis of phosphoryl transfer reactions. Its conservation across both protein and RNA enzymes spotlights it as a robust and efficient evolutionary solution to a fundamental biochemical challenge. However, our understanding of this mechanism has evolved from a simple static picture to a far more dynamic and nuanced view.

Monovalent cations have emerged from the background to be recognized as integral components of the catalytic machinery in many systems, generating a paradigm shift in our understanding of their role. The line between "structural" and "catalytic" ions is increasingly blurred, revealing a sophisticated hierarchy of dynamic ionic interactions that collectively shape the active site. Computational chemistry has matured into an equal partner with experiment in the field of mechanistic enzymology. Simulations provide the crucial dynamic context to static structures, enabling the visualization of reaction pathways, the calculation of energy barriers, and the dissection of the roles of individual ions and residues. The tight integration of high-resolution structural biology, biochemistry, and high-performance computing now represents the gold standard for mechanistic investigation. These findings showcased in this review underscore how combining all-atom simulations with experiments can resolve microscopic chemical mechanisms in complex environments where tightly or loosely bound metal ions play an increasingly critical role.

Declaration of competing interest

The authors declare that they have no known competing financial interests or personal relationships that could have appeared to influence the work reported in this paper.

Acknowledgments

JB thanks the Slovenian Research and Innovation Agency (ARIS) for financial support (Grant: P1-0017). AM thanks the financial support of the Italian Association for Cancer Research (AIRC IG grant 24514), and the Next Generation EU project PRIN 2022 (2022Z4FZE9 and CUP: B53D23004670006). AM and JA thank PNRR: National Center for Gene Therapy and Drugs based on RNA Technology CUP B83C22002860006 CN_0000004.

Data availability

No data was used for the research described in the article.

References

[1] T.R. Cech, Structural biology - the ribosome is a ribozyme, Science 289 (2000) 878–879, https://doi.org/10.1126/science.289.5481.878.
[2] G. Palermo, A. Cavalli, M.L. Klein, M. Alfonso-Prieto, M. Dal Peraro, M. De Vivo, Catalytic metal ions and enzymatic processing of DNA and RNA, Acc. Chem. Res. 48 (2015) 220–228, https://doi.org/10.1021/ar500314j.
[3] W. Yang, J.Y. Lee, M. Nowotny, Making and breaking nucleic acids: two-Mg2+−ion catalysis and substrate specificity, Mol. Cell 22 (2006) 5–13, https://doi.org/10.1016/j.molcel.2006.03.013.
[4] T.A. Steitz, J.A. Steitz, A general two-metal-ion mechanism for catalytic RNA, Proc. Natl. Acad. Sci. U. S. A. 90 (1993) 6498–6502, https://doi.org/10.1073/pnas.90.14.6498.
[5] T.A. Steitz, DNA polymerases: structural diversity and common mechanisms, J. Biol. Chem. 274 (1999) 17395–17398, https://doi.org/10.1074/jbc.274.25.17395.

[6] M. Nowotny, S.A. Gaidamakov, R.J. Crouch, W. Yang, Crystal structures of RNase H bound to an RNA/DNA hybrid: substrate specificity and metal-dependent catalysis, Cell 121 (2005) 1005–1016, https://doi.org/10.1016/j.cell.2005.04.024.
[7] W. Yang, Nucleases: diversity of structure, function and mechanism, Q. Rev. Biophys. 44 (2011) 1–93, https://doi.org/10.1017/S0033583510000181.
[8] M.R. Stahley, S.A. Strobel, Structural evidence for a two-metal-ion mechanism of group I intron splicing, Science 309 (2005) 1587–1590, https://doi.org/10.1126/science.1114994.
[9] N. Toor, K.S. Keating, S.D. Taylor, A.M. Pyle, Crystal structure of a self-spliced group II intron, Science 320 (2008) 77–82, https://doi.org/10.1126/science.1153803.
[10] J. Sgrignani, A. Magistrato, The structural role of Mg2+ ions in a class I RNA polymerase ribozyme: a molecular simulation study, J. Phys. Chem. B 116 (2012) 2259–2268, https://doi.org/10.1021/jp206475d.
[11] S.M. Fica, K. Nagai, Cryo-electron microscopy snapshots of the spliceosome: structural insights into a dynamic ribonucleoprotein machine, Nat. Struct. Mol. Biol. 24 (2017) 791–799, https://doi.org/10.1038/nsmb.3463.
[12] W.P. Galej, M.E. Wilkinson, S.M. Fica, C. Oubridge, A.J. Newman, K. Nagai, Cryo-EM structure of the spliceosome immediately after branching, Nature 537 (2016) 197–201, https://doi.org/10.1038/nature19316.
[13] P. Pokorna, J. Aupic, S.M. Fica, A. Magistrato, Decoding spliceosome dynamics through computation and experiment, Chem. Rev. 125 (2025) 9807–9833, https://doi.org/10.1021/acs.chemrev.5c00374.
[14] P.F. Lan, M. Tan, Y.B. Zhang, S.S. Niu, J. Chen, S.H. Shi, S.W. Qiu, X. Wang, X. D. Peng, G. Cai, H. Cheng, J. Wu, G.H. Li, M. Lei, Structural insight into precursor tRNA processing by yeast ribonuclease P, Science 362 (2018) 657, https://doi.org/10.1126/science.aat6678.
[15] P.F. Lan, B. Zhou, M. Tan, S.B. Li, M. Cao, J. Wu, M. Lei, Structural insight into precursor ribosomal RNA processing by ribonuclease MRP, Science 369 (2020) 656–663, https://doi.org/10.1126/science.abc0149.
[16] M. Marcia, A.M. Pyle, Visualizing group II intron catalysis through the stages of splicing, Cell 151 (2012) 497–507, https://doi.org/10.1016/j.cell.2012.09.033.
[17] A.G. Cassano, V.E. Anderson, M.E. Harris, Understanding the transition states of phosphodiester bond cleavage: insights from heavy atom isotope effects, Biopolymers 73 (2004) 110–129, https://doi.org/10.1002/bip.10517.
[18] S. Basu, R.P. Rambo, J. Strauss-Soukup, J.H. Cate, A.R. Ferré-D'Amaré, S. A. Strobel, J.A. Doudna, A specific monovalent metal ion integral to the AA platform of the RNA tetraloop receptor, Nat. Struct. Mol. Biol. 5 (1998) 986–992, https://doi.org/10.1038/2960.
[19] L. Casalino, A. Magistrato, Structural, dynamical and catalytic interplay between Mg2+ ions and RNA. Vices and virtues of atomistic simulations, Inorg. Chim. Acta 452 (2016) 73–81, https://doi.org/10.1016/j.ica.2016.02.011.
[20] M.E. Wilkinson, S.M. Fica, W.P. Galej, K. Nagai, Structural basis for conformational equilibrium of the catalytic spliceosome, Mol. Cell 81 (2021) 1439–1452, https://doi.org/10.1016/j.molcel.2021.02.021.
[21] J. Borisek, J. Aupic, A. Magistrato, Establishing the catalytic and regulatory mechanism of RNA-based machineries, Wiley Interdiscip. Rev. Comput. Mol. Sci. 13 (2023), https://doi.org/10.1002/wcms.1643.
[22] P. Auffinger, E. Ennifar, L. D'Ascenzo, Deflating the RNA Mg bubble: stereochemistry to the rescue!, RNA 27 (2021) 243–252, https://doi.org/10.1261/rna.076067.120.
[23] J. Aupič, J. Borišek, S.M. Fica, W.P. Galej, A. Magistrato, Monovalent metal ion binding promotes the first transesterification reaction in the spliceosome, Nat. Commun. 14 (2023) 8482, https://doi.org/10.1038/s41467-023-44174-2.
[24] P. Vidossich, A. Magistrato, QM/MM molecular dynamics studies of metal binding proteins, Biomolecules 4 (2014) 616–645, https://doi.org/10.3390/biom4030616.
[25] A. Warshel, Computer simulations of enzyme catalysis: methods, progress, and insights, Annu. Rev. Biophys. Biomol. Struct. 32 (2003) 425–443, https://doi.org/10.1146/annurev.biophys.32.110601.141807.
[26] M.W. van der Kamp, A.J. Mulholland, Combined quantum mechanics/molecular mechanics (QM/MM) methods in computational enzymology, Biochemistry (Mosc.) 52 (2013) 2708–2728, https://doi.org/10.1021/bi400215w.
[27] S.A. Adcock, J.A. McCammon, Molecular dynamics: survey of methods for simulating the activity of proteins, Chem. Rev. 106 (2006) 1589–1615, https://doi.org/10.1021/cr040426m.
[28] J. Sponer, G. Bussi, M. Krepl, P. Banas, S. Bottaro, R.A. Cunha, A. Gil-Ley, G. Pinamonti, S. Poblete, P. Jureacka, N.G. Walter, M. Otyepka, RNA structural dynamics as captured by molecular simulations: a comprehensive overview, Chem. Rev. 118 (2018) 4177–4338, https://doi.org/10.1021/acs.chemrev.7b00427.
[29] W.F. van Gunsteren, X. Daura, N. Hansen, A.E. Mark, C. Oostenbrink, S. Riniker, L.J. Smith, Validation of molecular simulation: an overview of issues, Angew. Chem. Int. Ed. 57 (2018) 884–902, https://doi.org/10.1002/anie.201702945.
[30] A. Laio, M. Parrinello, Escaping free-energy minima, Proc. Natl. Acad. Sci. U. S. A. 99 (2002) 12562–12566, https://doi.org/10.1073/pnas.202427399.
[31] G.M. Torrie, J.P. Valleau, Nonphysical sampling distributions in Monte Carlo free-energy estimation: umbrella sampling, J. Comput. Phys. 23 (1977) 187–199, https://doi.org/10.1016/0021-9991(77)90121-8.
[32] T.P. Straatsma, J.A. Mccammon, Computational alchemy, Annu. Rev. Phys. Chem. 43 (1992) 407–435, https://doi.org/10.1146/annurev.pc.43.100192.002203.
[33] Y. Sugita, Y. Okamoto, Replica-exchange molecular dynamics method for protein folding, Chem. Phys. Lett. 314 (1999) 141–151, https://doi.org/10.1016/S0009-2614(99)01123-9.
[34] Y.I. Yang, Q. Shao, J. Zhang, L.J. Yang, Y.Q. Gao, Enhanced sampling in molecular dynamics, J. Chem. Phys. 151 (2019) 070902, https://doi.org/10.1063/1.5109531.
[35] M. Invernizzi, P.M. Piaggi, M. Parrinello, Unified approach to enhanced sampling, Phys. Rev. X 10 (2020) 041034, https://doi.org/10.1103/PhysRevX.10.041034.
[36] P. Janoš, A. Spinello, A. Magistrato, All-atom simulations to studying metallodrugs/target interactions, Curr. Opin. Chem. Biol. 61 (2020) 1–8, https://doi.org/10.1016/j.cbpa.2020.07.005.
[37] Q. Cui, Perspective: quantum mechanical methods in biochemistry and biophysics, J. Chem. Phys. 145 (2016) 140901, https://doi.org/10.1063/1.4964410.
[38] E. Brunk, U. Rothlisberger, Mixed quantum mechanical/molecular mechanical molecular dynamics simulations of biological Systems in Ground and Electronically Excited States, Chem. Rev. 115 (2015) 6217–6263, https://doi.org/10.1021/cr500628b.
[39] H.M. Senn, W. Thiel, QM/MM methods for biomolecular systems, Angew. Chem. Int. Ed. 48 (2009) 1198–1229, https://doi.org/10.1002/anie.200802019.
[40] M. Sprik, G. Ciccotti, Free energy from constrained molecular dynamics, J. Chem. Phys. 109 (1998) 7737–7744, https://doi.org/10.1063/1.477419.
[41] L. Casalino, G. Palermo, U. Rothlisberger, A. Magistrato, Who activates the nucleophile in ribozyme catalysis? An answer from the splicing mechanism of group II introns, J. Am. Chem. Soc. 138 (2016) 10374–10377, https://doi.org/10.1021/jacs.6b01363.
[42] F.H. Westheimer, Why nature chose phosphates, Science 235 (1987) 1173–1178, https://doi.org/10.1126/science.2434996.
[43] C.M. Joyce, T.A. Steitz, Function and structure relationships in DNA-polymerases, Annu. Rev. Biochem. 63 (1994) 777–822, https://doi.org/10.1146/annurev.biochem.63.1.777.
[44] T. Nakamura, Y. Zhao, Y. Yamagata, Y.J. Hua, W. Yang, Mechanism of the nucleotidyl-transfer reaction in DNA polymerase revealed by time-resolved protein crystallography, Biophysics 9 (2013) 31–36, https://doi.org/10.2142/biophysics.9.31.
[45] A.M. Pyle, Metal ions in the structure and function of RNA, J. Biol. Inorg. Chem. 7 (2002) 679–690, https://doi.org/10.1007/s00775-002-0387-6.
[46] J.E. Wedekind, Metal ion binding and function in natural and artificial small RNA enzymes from a structural perspective, Met. Ions Life Sci. 9 (2011) 299–345, https://doi.org/10.1039/9781849732512002 99.
[47] C. Yan, R. Wan, Y. Shi, Molecular mechanisms of pre-mRNA splicing through structural biology of the spliceosome, Cold Spring Harb. Perspect. Biol. 11 (2019) a032409, https://doi.org/10.1101/cshperspect.a032409.
[48] Y. Gao, W. Yang, Capture of a third Mg2+ is essential for catalyzing DNA synthesis, Science 352 (2016) 1334–1337, https://doi.org/10.1126/science.aad9633.
[49] D.R. Stevens, S. Hammes-Schiffer, Exploring the role of the third active site metal ion in DNA polymerase η with QM/MM free energy simulations, J. Am. Chem. Soc. 140 (2018) 8965–8969, https://doi.org/10.1021/jacs.8b05177.
[50] V. Genna, P. Vidossich, E. Ippoliti, P. Carloni, M. De Vivo, A self-activated mechanism for nucleic acid polymerization catalyzed by DNA/RNA polymerases, J. Am. Chem. Soc. 138 (2016) 14592–14598, https://doi.org/10.1021/jacs.6b05475.
[51] L. Perera, B.D. Freudenthal, W.A. Beard, D.D. Shock, L.G. Pedersen, S.H. Wilson, Requirement for transient metal ions revealed through computational analysis for DNA polymerase going in reverse, Proc. Natl. Acad. Sci. U. S. A. 112 (2015) E5228–E5236, https://doi.org/10.1073/pnas.1511207112.
[52] L. Perera, B.D. Freudenthal, W.A. Beard, L.G. Pedersen, S.H. Wilson, Revealing the role of the product metal in DNA polymerase β catalysis, Nucleic Acids Res. 45 (2017) 2736–2745, https://doi.org/10.1093/nar/gkw1363.
[53] M.M. Pedroso, J.A. Larrabee, F. Ely, S.E. Gwee, N. Mitic, D.L. Ollis, L.R. Gahan, G. Schenk, CaII binding regulates and dominates the reactivity of a transition-metal-ion-dependent Diesterase from mycobacterium tuberculosis, Chem. A Eur. J. 22 (2016) 999–1009, https://doi.org/10.1002/chem.201504001.
[54] R. Molina, S. Stella, P. Redondo, H. Gomez, M.J. Marcaida, M. Orozco, J. Prieto, G. Montoya, Visualizing phosphodiester-bond hydrolysis by an endonuclease, Nat. Struct. Mol. Biol. 22 (2015) 65–72, https://doi.org/10.1038/nsmb.2932.
[55] W. Hwang, J. Yoo, Y. Lee, S. Park, P.L. Hoang, H. Cho, J. Yu, T.M.H. Vo, M. S. Shin, M.S. Jin, D. Park, C. Hyeon, G. Lee, Dynamic coordination of two-metal-ions orchestrates λ-exonuclease catalysis, Nat. Commun. 9 (2018) 4404, https://doi.org/10.1038/s41467-018-06750-9.
[56] C.K.M. Tse, J. Xu, L. Xu, F.K. Sheong, S.L. Wang, H.Y. Chow, X. Gao, X.C. Li, P.P. H. Cheung, D. Wang, Y.K. Zhang, X.H. Huang, Intrinsic cleavage of RNA polymerase II adopts a nucleobase-independent mechanism assisted by transcript phosphate, Nat. Catal. 2 (2019) 228–235, https://doi.org/10.1038/s41929-019-0227-5.
[57] M. Roca, Y. Maghsoud, G.A. Cisneros, K. Swiderek, V. Moliner, Comparing force field treatments in QM/MM studies of the SARS-CoV-2 RNA-dependent RNA polymerase (RdRp) mechanism, J. Chem. Theory Comput. 21 (2025) 12342–12355, https://doi.org/10.1021/acs.jctc.5c01399.
[58] J. Borisek, J. Aupic, A. Magistrato, Third metal ion dictates the catalytic activity of the two-metal-ion pre-ribosomal RNA-processing machinery, Angew. Chem. Int. Ed. 63 (2024) e202405819, https://doi.org/10.1002/anie.202405819.
[59] V. Genna, M. Colombo, M. De Vivo, M. Marcia, Second-Shell basic residues expand the two-metal-ion architecture of DNA and RNA processing enzymes, Structure 26 (2018) 40–50, https://doi.org/10.1016/j.str.2017.11.008.
[60] D.E. Draper, A guide to ions and RNA structure, RNA 10 (2004) 335–343, https://doi.org/10.1261/rna.5205404.

[61] Z.J. Tan, S.J. Chen, Nucleic acid helix stability: effects of salt concentration, cation valence and size, and chain length, Biophys. J. 90 (2006) 1175–1190, https://doi.org/10.1529/biophysj.105.070904.
[62] M. Anderson, E.P. Schultz, M. Martick, W.G. Scott, Active-site monovalent cations revealed in a 1.55-Å-resolution hammerhead ribozyme structure, J. Mol. Biol. 425 (2013) 3790–3798, https://doi.org/10.1016/j.jmb.2013.05.017.
[63] H. Nishimasu, S. Fushinobu, H. Shoun, T. Wakagi, The first crystal structure of the novel class of fructose-1,6-bisphosphatase present in thermophilic archaea, Structure 12 (2004) 949–959, https://doi.org/10.1016/j.str.2004.03.026.
[64] F. Leonarski, L. D'Ascenzo, P. Auffinger, Nucleobase carbonyl groups are poor Mg inner-sphere binders but excellent monovalent ion binders-a critical PDB survey, RNA 25 (2019) 173–192, https://doi.org/10.1261/rna.068437.118.
[65] N.L. Samara, W. Yang, Cation trafficking propels RNA hydrolysis, Nat. Struct. Mol. Biol. 25 (2018) 715–721, https://doi.org/10.1038/s41594-018-0099-4.
[66] K.A. Senn, K.A. Lipinski, N.J. Zeps, A.F. Griffin, M.E. Wilkinson, A.A. Hoskins, Control of 3′ splice site selection by the yeast splicing factor Fyv6, Elife 13 (2024) e1643, https://doi.org/10.7554/eLife.100449.
[67] D.W. Gohara, E. Di Cera, Molecular mechanisms of enzyme activation by monovalent cations, J. Biol. Chem. 291 (2016) 20840–20848, https://doi.org/10.1074/jbc.R116.737833.
[68] S. Ekesan, E. McCarthy, D.A. Case, D.M. York, RNA electrostatics: how ribozymes engineer active sites to enable catalysis, J. Phys. Chem. B 126 (2022) 5982–5990, https://doi.org/10.1021/acs.jpcb.2c03727.
[69] J. Manigrasso, M. De Vivo, G. Palermo, Controlled trafficking of multiple and diverse cations prompts nucleic acid hydrolysis, ACS Catal. 11 (2021) 8786–8797, https://doi.org/10.1021/acscatal.1c01825.
[70] V. Genna, R. Gaspari, M. Dal Peraro, M. De Vivo, Cooperative motion of a key positively charged residue and metal ions for DNA replication catalyzed by human DNA polymerase-eta, Nucleic Acids Res. 44 (2016) 2827–2836, https://doi.org/10.1093/nar/gkw128.
[71] M. De Vivo, M. Dal Peraro, M.L. Klein, Phosphodiester cleavage in ribonuclease H occurs via an associative two-metal-aided catalytic mechanism, J. Am. Chem. Soc. 130 (2008) 10955–10962, https://doi.org/10.1021/ja8005786.
[72] E. Rosta, M. Nowotny, W. Yang, G. Hummer, Catalytic mechanism of RNA backbone cleavage by ribonuclease H from quantum mechanics/molecular mechanics simulations, J. Am. Chem. Soc. 133 (2011) 8934–8941, https://doi.org/10.1021/ja200173a.
[73] J. Sgrignani, A. Magistrato, QM/MM MD simulations on the enzymatic pathway of the human flap endonuclease (hFEN1) elucidating common cleavage pathways to RNase H enzymes, ACS Catal. 5 (2015) 3864–3875, https://doi.org/10.1021/acscatal.5b00178.
[74] L. Casalino, Ł. Nierzwicki, M. Jinek, G. Palermo, Catalytic mechanism of non-target DNA cleavage in CRISPR-Cas9 revealed by ab initio molecular dynamics, ACS Catal. 10 (2020) 13596–13605, https://doi.org/10.1021/acscatal.0c03566.
[75] A. Roy, G.A. Cisneros, Comparison of magnesium and manganese ions on the structural and catalytic properties of human DNA polymerase gamma, J. Chem. Theory Comput. 21 (2025) 9094–9106, https://doi.org/10.1021/acs.jctc.5c00435.
[76] D. Berta, P.J. Buigues, M. Badaoui, E. Rosta, Cations in motion: QM/MM studies of the dynamic and electrostatic roles of hand Mg ions in enzyme reactions, Curr. Opin. Struct. Biol. 61 (2020) 198–206, https://doi.org/10.1016/j.sbi.2020.01.002.
[77] A. Ganguly, P. Thaplyal, E. Rosta, P.C. Bevilacqua, S. Hammes-Schiffer, Quantum mechanical/molecular mechanical free energy simulations of the self-cleavage reaction in the hepatitis delta virus ribozyme, J. Am. Chem. Soc. 136 (2014) 1483–1496, https://doi.org/10.1021/ja4104217.
[78] W.B. Lott, B.W. Pontius, P.H. von Hippel, A two-metal ion mechanism operates in the hammerhead ribozyme-mediated cleavage of an RNA substrate, Proc. Natl. Acad. Sci. U. S. A. 95 (1998) 542–547, https://doi.org/10.1073/pnas.95.2.542.
[79] D. Roston, D. Demapan, Q. Cui, Extensive free-energy simulations identify water as the base in nucleotide addition by DNA polymerase, Proc. Natl. Acad. Sci. U. S. A. 116 (2019) 25048–25056, https://doi.org/10.1073/pnas.1914613116.
[80] E. Rosta, W. Yang, G. Hummer, Calcium inhibition of ribonuclease H1 two-metal ion catalysis, J. Am. Chem. Soc. 136 (2014) 3137–3144, https://doi.org/10.1021/ja411408x.
[81] W.T. Huang, Y. Huang, J. Xu, J.L. Liao, How does the spliceosome catalyze intron lariat formation? Insights from quantum mechanics/molecular mechanics free-energy simulations, J. Phys. Chem. B 123 (2019) 6049–6055, https://doi.org/10.1021/acs.jpcb.9b04377.
[82] S.M. Fica, N. Tuttle, T. Novak, N.S. Li, J. Lu, P. Koodathingal, Q. Dai, J.P. Staley, J.A. Piccirilli, RNA catalyses nuclear pre-mRNA splicing, Nature 503 (2013) 229–234, https://doi.org/10.1038/nature12734.
[83] A. Perederina, D. Li, H. Lee, C. Bator, I. Berezin, S.L. Hafenstein, A.S. Krasilnikov, Cryo-EM structure of catalytic ribonucleoprotein complex RNase MRP, Nat. Commun. 11 (2020) 1–10, https://doi.org/10.1038/s41467-020-17308-z.
[84] S.O. Shan, A. Yoshida, S.G. Sun, J.A. Piccirilli, D. Herschlag, Three metal ions at the active site of the group I ribozyme, Proc. Natl. Acad. Sci. U. S. A. 96 (1999) 12299–12304, https://doi.org/10.1073/pnas.96.22.12299.
[85] S.L. Dürr, O. Bohuszewicz, D. Berta, R. Suardiaz, P.G. Jambrina, C. Peter, Y. H. Shao, E. Rosta, The role of conserved residues in the DEDDh motif: the proton-transfer mechanism of HIV-1 RNase H, ACS Catal. 11 (2021) 7915–7927, https://doi.org/10.1021/acscatal.1c01493.
[86] J. Borišek, A. Magistrato, All-atom simulations decrypt the molecular terms of RNA catalysis in the exon-ligation step of the spliceosome, ACS Catal. 10 (2020) 5328–5334, https://doi.org/10.1021/acscatal.0c00390.
[87] E. Posani, P. Janos, D. Haack, N. Toor, M. Bonomi, A. Magistrato, G. Bussi, Ensemble refinement of mismodeled cryo-EM RNA structures using all-atom simulations, Nat. Commun. 16 (2025) 4549, https://doi.org/10.1038/s41467-025-59769-0.
[88] L. Shub, W.J. Liu, G. Skiniotis, M.J. Keiser, M.J. Robertson, MIC: a deep learning tool for assigning ions and waters in cryo-EM and crystal structures, Nat. Commun. 16 (2025) 6182, https://doi.org/10.1038/s41467-025-61315-x.
[89] K. Wang, Z.D. Yin, C.J. Sang, W.T. Xia, Y. Wang, T.T. Sun, X.J. Xu, Geometric deep learning for the prediction of magnesium-binding sites in RNA structures, Int. J. Biol. Macromol. 262 (2024) 130150, https://doi.org/10.1016/j.ijbiomac.2024.130150.
[90] Y. Zhou, S.-J. Chen, Graph deep learning locates magnesium ions in RNA, QRB Discovery 3 (2022) e20, https://doi.org/10.1017/qrd.2022.17.
[91] N. Naleem, A. Henning-Knechtel, S. Kirmizialtin, P. Auffinger, Cat_wiz: a stereochemistry-guided toolkit for locating, diagnosing and annotating Mg2+ ions in RNA structures, bioRxiv (2025) 2025.2010.2004.677962, doi:https://doi.org/10.1101/2025.10.04.677962.
[92] L. Casalino, G. Palermo, N. Abdurakhmonova, U. Rothlisberger, A. Magistrato, Development of site-specific Mg2+-RNA force field parameters: a dream or reality? Guidelines from combined molecular dynamics and quantum mechanics simulations, J. Chem. Theory Comput. 13 (2017) 340–352, https://doi.org/10.1021/acs.jctc.6b00905.
[93] J.A. Lemkul, A.D. MacKerell, Polarizable force field for RNA based on the classical drude oscillator, J. Comput. Chem. 39 (2018) 2624–2646, https://doi.org/10.1002/jcc.25709.
[94] G.A. Cisneros, M. Karttunen, P.Y. Ren, C. Sagui, Classical Electrostatics for biomolecular simulations, Chem. Rev. 114 (2014) 779–814, https://doi.org/10.1021/cr300461d.
[95] J.W. Ponder, C.J. Wu, P.Y. Ren, V.S. Pande, J.D. Chodera, M.J. Schnieders, I. Haque, D.L. Mobley, D.S. Lambrecht, R.A. DiStasio, M. Head-Gordon, G.N. I. Clark, M.E. Johnson, T. Head-Gordon, Current status of the AMOEBA polarizable force field, J. Phys. Chem. B 114 (2010) 2549–2564, https://doi.org/10.1021/jp910674d.
[96] F. Noé, A. Tkatchenko, K.R. Müller, C. Clementi, Machine learning for molecular simulation, Annu. Rev. Phys. Chem. 71 (2020) 361–390, https://doi.org/10.1146/annurev-physchem-042018-052331.
[97] O.T. Unke, S. Chmiela, H.E. Sauceda, M. Gastegger, I. Poltaysky, K.T. Schütt, A. Tkatchenko, K.R. Müller, Machine learning force fields, Chem. Rev. 121 (2021) 10142–10186, https://doi.org/10.1021/acs.chemrev.0c01111.
[98] J.S. Smith, O. Isayev, A.E. Roitberg, ANI-1: an extensible neural network potential with DFT accuracy at force field computational cost, Chem. Sci. 8 (2017) 3192–3203, https://doi.org/10.1039/c6sc05720a.
[99] G.R. Bowman, P.L. Geissler, Equilibrium fluctuations of a single folded protein reveal a multitude of potential cryptic allosteric sites, Proc. Natl. Acad. Sci. U.S A. 109 (2012) 11681–11686, https://doi.org/10.1073/pnas.1209309109.
[100] M.D. Disney, Targeting RNA with small molecules to capture opportunities at the intersection of chemistry, biology, and medicine, J. Am. Chem. Soc. 141 (2019) 6776–6790, https://doi.org/10.1021/jacs.8b13419.
[101] S.D. Veenbaas, J.T. Koehn, P.S. Irving, N.N. Lama, K.M. Weeks, Ligand- binding pockets in RNA and where to find them, Proc. Natl. Acad. Sci. U. S. A. 122 (2025) e2422346122, https://doi.org/10.1073/pnas.2422346122.